Title
Low Temperature Sulfur Deposition for High-Performance Lithium/Sulfur Cells

Journal
Journal of The Electrochemical Society, 165(9)

ISSN
0013-4651

Authors
Kawase, Ayako
Han, Don Donghyeok
Cairns, Elton J

Publication Date
2018

DOI
10.1149/2.1051809jes

Peer reviewed

Low temperature sulfur deposition for high-performance Lithium/Sulfur Cells

Ayako Kawase[a], *Don Donghyeok Han*[b] *and Elton J. Cairns*[a,b]*

a. Energy Storage and Distributed Resources Division, Lawrence Berkeley National Laboratory, Berkeley, CA 94720, USA

b. Department of Chemical and Biomolecular Engineering, University of California, Berkeley, CA 94720, USA

Corresponding Author

* Elton J. Cairns

Energy Storage and Distributed Resources Division, Lawrence Berkeley National Laboratory, and Department of Chemical and Biomolecular Engineering, University of California, Berkeley

ejcairns@lbl.gov

ABSTRACT: Sulfur deposition is an effective method for creating composites of sulfur with various conductive materials. In this study we investigated the details of the deposition process of sulfur onto graphene oxide (GO). It was revealed that just mixing a polysulfide solution and a GO suspension resulted in the deposition of sulfur onto the GO under alkaline conditions. The combination of the alkaline deposition and subsequent acidic deposition at —different temperatures yielded materials with various morphologies. The sulfur deposition rate influenced the morphology of the S deposit and the resulting Li/S cell performance. By controlling the process with a moderate time for the alkaline deposition and subsequent acidic deposition at a decreased temperature, a preferred morphology of the sulfur/GO composite with a high sulfur utilization was successfully synthesized. This preferred morphology of SGO provides for a high-performance Li/S cell.

KEYWORDS: Sulfur, Graphene oxide, CTAB, Lithium

1. Introduction:

The research of lithium/sulfur cells with high theoretical specific energy has been active in the development of next-generation rechargeable batteries. Lithium/sulfur cells are also attractive because sulfur is an abundant, harmless natural resource and low in cost. However, there are still challenges for the practical application such as low sulfur utilization due to sulfur's insulating properties and capacity degradation resulting from dissolution-precipitation or the polysulfide redox shuttle phenomenon. Additional approaches to overcome these shortcomings of the lithium/sulfur cell are in high demand.

In order to enhance the cell performance, a wide variety of composites with sulfur and various conductive materials have been proposed [1-14]. Although a number of methodologies have been proposed, one major method to fabricate such composites is to infiltrate molten sulfur into cavities of the conductive material by heating the mixture above 115 °C (155°C is commonly used). Another significant technique is chemical deposition of sulfur onto conductive materials [8-14]. Of course, the structures of the composites are influenced by the structure of the original conductive materials, but the resulting structure is also significantly affected by the method of sulfur deposition.

In recent works, a composite of sulfur and graphene oxide (GO) has exhibited excellent cell performance with a high initial discharge capacity and high rate capability up to 6C while still maintaining high specific capacity (e.g., 800mA·h/g (sulfur) at 6C) [1]. The cells also demonstrated durability up to 1500 cycles with a low capacity decay rate [1]. The synthesis of the material consisted of chemical deposition of sulfur onto GO by acidification of a polysulfide solution and subsequent heat treatment. The previous studies revealed that CTAB (cetyltrimethylammoniumbromide) interacted with sulfur not only as a surfactant but also as a

protection layer because of the newly created compounds by chemical reactions between CTAB and polysulfide during the heat treatment process [7]. In order to create a practical cell, a water-based synthesis process of the composite is favorable because it is environmentally friendly and it can be easily scaled up. Controlling the process is necessary for designing the scale-up of active material preparation and optimization of cell performance and lifetime. Furthermore, ~~Although it has been revealed that these reactions during the heat treatment improved the cell performance, a detailed investigation of the sulfur deposition process has not been conducted. N~~not only for improvement of the sulfur/GO materials, but also for creation of new sulfur composites, a deep understanding of the deposition process of sulfur is indispensable.

In this study, the sulfur deposition process was investigated including the mixing process of polysulfide and GO and the acidification process. The influence of each step and the conditions under which it is performed on the composite morphology and the cell performance have been clarified by using elemental analysis (EA), i.e. CHNS analysis, scanning electron microscopy (SEM), and electrochemical characterization.

2. Materials and Methods:

2.1 Synthesis:

SGO-Mx (x is a variable representing the mixing time in hours) samples: 0.29 g sodium sulfide (Na_2S, anhydrous, Alfa Aesar) was dissolved in 12.5 mL distilled water to form a Na_2S solution. 0.36 g elemental sulfur (99.5%, Alfa Aesar) was dissolved in the Na_2S solution to form a sodium polysulfide (Na_2S_x) solution after stirring for 4 hours at 70 °C. 12 ml commercial GO-water dispersion (4 mg/mL, Graphenea) was diluted with water to form 78 ml of suspension and sonicated for 1.5 hours. The flake size of the original GO was 32.9 □m at D90, 16.6 □m at D50

and 6.63 μm at D10 from the information provided by the manufacturer of the GO. 82 mg CTAB (2.5 mM in the GO suspension, Sigma Aldrich) was dissolved in 3 mL water and added to the GO suspension drop-wise and stirred and sonicated for 1.5 hours. Then, the Na_2S_x solution was added to the as-prepared GO-CTAB suspension drop-wise. The Na_2S_x-GO-CTAB mixture was stirred for a different amount of time for each experiment. The mixing time, i. e. alkaline deposition time, for each sample is listed in Table 1. The powder was filtered and washed with acetone and water, and dried at 45 °C in a vacuum oven for 12 hours.

SGO-Mx-Ay (y is a variable representing the acidification temperature) samples: The same procedure was used before the filtration as for the SGO-Mx samples. The mixture was slowly added to 50 mL of 2 M formic acid solution (Aldrich) and the mixture was stirred until the solution phase became clear from a milky colloidal suspension at different temperatures for each experiment. Then the powder was filtered and washed with acetone and water, and dried at 45 °C in a vacuum oven for 12 hours.

SGO-Mx-Ay-H samples: After drying, the sample was heated (heat treatment) in a tube furnace at 155 °C for 18 hours under Ar with a flow rate of 100 cc/min. An alumina boat containing the sample powders was wrapped with aluminum foil to prevent sulfur evaporation.

The obtained samples are labeled as listed in Table 1.

2.2 Material characterization:

Elemental analysis was performed using a Perkin Elmer 2400 CHNS/O series II analyzer. Combustion and reduction temperatures were 975 °C and 500 °C, respectively. The combustion parameters were 2, 10, 0, 0. The content of oxygen was estimated by the difference between 100% and the sum total of the contents of carbon, hydrogen, nitrogen and sulfur based on the

assumption that there was no other element than carbon, hydrogen, nitrogen, sulfur and oxygen comprising the composition of the starting materials. The sodium in sodium sulfide should have been washed out when the powder samples were washed with water and acetone.

SEM observation was conducted using Zeiss Gemini Ultra-55 Analytical Field Emission Scanning Electron Microscope. A secondary electron detector was used. The EDS system was used for elemental x-ray analysis. The beam energy was 5 kV with 1 nm resolution.

2.3 Electrochemical characterization:

The sulfur electrodes were fabricated by mixing the samples after the heat treatment, carbon black (Super P C65) with a binder (SBR/CMC 1:1 by weight) at a weight ratio of 70:20:10 in isopropanol/water (1:3 by volume) solution to form a slurry. The resulting slurry was uniformly spread via a doctor blade onto pure aluminum foil. The solvent was allowed to evaporate at room temperature for 24 hours. The electrode was punched into circular pieces with a diameter of 12.7 mm for assembly into coin cells. The electrodes were then dried in a vacuum oven at 50 °C for 24 hours to eliminate any solvent residue. The sulfur content of the cathodes was 59% as a result of having 84% sulfur in the active materials and 70% active materials in the cathodes. The average sulfur loading of the electrodes was ~0.8mg/cm^2. For the electrolyte, 1 mol/kg lithium bis(trifluoromethylsulfonyl)imide (Sigma-Aldrich) in (N-methyl-(N-butyl) pyrrolidinium bis(trifluoromethanesulfonyl)imide (Sigma-Aldrich) / 1,3-dioxolane / 1,2-dimethoxyethane mixture (2:1:1, by volume) was prepared. 50 µL of the electrolyte ~~and~~was used for evaluation of the electrochemical performance. 0.25 mol/kg $LiNO_3$ was used as an additive in the electrolyte.

Type CR2032 coin cells were assembled with a separator (Celgard 2400) between a lithium metal foil (99.98%, Cyprus Foote Mineral) and a sulfur electrode fabricated with the SGO-Mx-

Ay-H active material in a glove box filled with argon gas. Galvanostatic discharge and charge testing of the coin cells was performed using a battery cycler (Maccor Series 4000) at the 0.2 C rate (1 C = 1675 mA/g (sulfur)) for discharge and 0.1 C rate for charge between 1.7 and 2.8V. Then the current was changed accordingly. The cell capacity was normalized by the weight of sulfur. All electrochemical characterizations were performed at 30 °C. Before all electrochemical characterizations, the cells were held at open circuit at 30 °C for 12 h.

3. Results and Discussion:

Chemical deposition of elemental sulfur takes place from a S_x^{2-} precursor under acid conditions. The reaction occurs because the equilibrium of polysulfide and sulfur shifts toward sulfur as the pH decreases. The equilibrium between elemental sulfur and polysulfide under acid conditions can be written as:

$$S_iS^{2-} + H^+ \Leftrightarrow iS_{(s)} + HS^- \quad (1)$$

The equilibrium under alkaline conditions can be written as Equation (2) as well [15].

$$S_iS^{2-} + H_2O \Leftrightarrow iS_{(s)} + HS^- + OH^- \quad (2)$$

In the preparation of the sulfur-GO composites, acidification with formic acid was introduced with the aim of obtaining elemental sulfur deposited on GO. The preparation of the sulfur-GO composites is shown graphically in Fig. 1. The first step is the mixing process of the Na_2S_x solution and the GO suspension. After mixing the Na_2S_x solution and the GO suspension, the mixture was added dropwise into the formic acid solution. During the acidification process, polysulfide was supposed to deposit on GO as elemental sulfur. In our earlier understanding, it was assumed that the mixing process of Na_2S_x and GO was just mixing of polysulfide and GO to make a homogeneous mixture. However, it was found that some chemical reactions were taking

place during the mixing process. Powder samples were taken from the suspension at different times. The powders prepared by mixing Na_2S_x and GO for 1 hour, 3 hours, 6 hours, 28 hours and 52 hours are labeled as SGO-M1, SGO-M3, SGO-M6, SGO-M16, SGO-M28 and SGO-M52 respectively. Each sample was analyzed to check the contents of carbon, hydrogen, nitrogen and sulfur by CHNS elemental analysis (shown in Fig. S1). The content of oxygen was estimated by the difference of 100% and the sum total of the contents of carbon, hydrogen, nitrogen and sulfur based on the assumption that there was no other element than carbon, hydrogen, nitrogen, sulfur and oxygen comprising the composition of the starting materials. The sodium in sodium sulfide should have been washed out when the powder samples were washed by water and acetone. The contents of sulfur and oxygen are indicated in Fig. 2 (a). The content of sulfur significantly increased with time until 28 hours and gradually saturated until 52 hours. At the point of 52 hours from starting, the content of sulfur was 77%. This means that sulfur deposited without any additional acid. As regards oxygen, the content was 57% in the original GO. These oxygen sources were from adsorbed water and surface functional groups containing oxygen [16]. The TGA result for GO also indicated corresponding weight loss of water and the functional groups as shown in Fig. S2 [16]. These oxygen-based functional groups are known to produce protons by deoxygenation [17]. This is the reason why the GO suspension is acidic. When the content of oxygen is tracked in Fig. 2 (a), it dropped down from 57% to 12% just after starting. Then the content decreased from 5.8% at 28 hours to 1.1% at 52 hours. This means GO was almost completely reduced to graphene with some defects after 52 hours.

The pH was monitored during the process. Fig. 2 (a) shows the pH change of the solution of Na_2S_x and GO. The initial pH of the polysulfide solution was 11.0, and the pH of the original GO suspension was from 2.7 to 3.1. Just after adding the polysulfide solution to the GO suspension,

the pH reached 11, and then decreased to around 9.7 taking about 6 hours. From this point, the pH gradually decreased to around 9.0 over a period of about 40 hours. At the point of 48 hours after starting, the pH started to drop drastically and reached 7.0 at 52 hours after starting. The color of the original polysulfide solution was dark orange. During the process, the color gradually became pale, and it turned to colorless when the pH started to drop down to 7.0 at 48 hours.

All these results indicate that polysulfides were gradually converted to elemental sulfur during the mixing time, and all of the polysulfide in the solution was consumed at 52 hours after starting. Regarding the change of the oxygen content, it can be assumed that polysulfides were oxidized to sulfur by protons produced from deoxygenation of GO. This phenomenon demonstrated sulfur deposition under alkaline conditions as represented in Equation (2). We call this alkaline deposition in contrast to the deposition under acidic conditions.

Fig. 2 (a) suggests that the deoxygenation rate of GO became slower after 6 hours. This phenomenon suggests that there are mainly two types of deoxygenation reactions on GO, one of them is fast and the other type is much slower. This is also supported by the literature offering different deoxygenation reactions in strongly alkaline conditions and mild alkaline conditions [17]. The model reactions are shown in Fig. S3. It can be presumed that the conductivity of the SGO material increased as the reduction of GO proceeded with time. ~~From these experiments, we found that alkaline deposition of sulfur occurred during the first step of the synthesis process, and a composite of sulfur and reduced GO was produced. The sulfur contents of those composites were different depending on the elapsed time of the process.~~

After the alkaline deposition during the mixing process, acidification using formic acid was conducted. The pH during the process was about 2.4. ~~The solution mixture of polysulfide and~~

~~GO was added dropwise to the formic acid solution.~~ In this process, the remaining polysulfide in the solution was supposed to be acidified to produce elemental sulfur according to Equation (1). We call it acidic deposition in contrast to the alkaline deposition described above. The sulfur contents of all the samples after the acidic deposition were 84% from the elemental analysis. When the polysulfide mixture was added to the formic acid solution, the color of the solution turned to milky blue gray immediately. Photos of the color change during the acidification are shown in Fig. S4. The origin of the milky color was a colloid of liquid sulfur particles created by polysulfide ~~which had not been converted to solid sulfur yet at this time~~ [18]. Then the milky ~~blue gray~~ color gradually ~~changed to more like milky black, and finally the milky solution~~ became clear. We define the time from starting to the time at which the solution becomes clear as the acidic deposition time. The acidic deposition times for samples prepared with different alkaline deposition times are shown in Fig. 2 (b). As expected from the result for the alkaline deposition, the remaining amount of polysulfide was different depending on the alkaline deposition time. Thus, the acidic deposition time after shorter alkaline deposition times was longer because more polysulfide remained after the shorter alkaline deposition times. The acidic deposition time after 1 hour of alkaline deposition was about 5 hours. Comparing with the total time needed for alkaline deposition to be completed, which was 52 hours, it is obvious that the acidic deposition is significantly faster than the alkaline deposition.

Upon a further investigation, it was found that the acidic deposition time was also influenced significantly by other factors. Fig. 2 (c) shows that the acidic deposition time increased linearly when more CTAB was added. ~~When no CTAB was used, the deposition quickly went to completion as sulfur particles rapidly deposited onto the graphene oxide surface.~~ This phenomenon was anticipated because liquid sulfur particles were expected to be more stabilized

with increased CTAB concentration, and thus took a longer time to destabilize and deposit onto the graphene surface [18].

Furthermore, the temperature dependency of the acidic deposition time was investigated, and the results are shown in Fig. 2 (d). The acidic deposition time was influenced strongly by temperature. Considering the fact that the solubility of CTAB is significantly influenced by temperature especially in the range from 10 °C to 50 °C [19], it was speculated that higher temperature increased CTAB solubility and that better stabilized the liquid sulfur particles as a colloid. The speculation was correct only above 15 °C. The acidic deposition time at 15 ˚C was found to be the shortest. The acidic deposition time increased at higher temperatures than 15 °C~~, and the acidic deposition at 50 ˚C did not go to completion even after overnight~~. The existence of the minimum suggests that there are additional factors associated with temperature that affect the deposition of sulfur other than CTAB solubility. One of the possibilities is that an increase in temperature may increase the deposition rate that counter balances the decreased deposition rate by CTAB-stabilized sulfur. This is reasonable with regard to the endothermic reaction of sulfur deposition.

The morphologies of the samples prepared using different alkaline deposition times and associated different acidic deposition times were investigated. Also, the effect of different acidic deposition conditions on the morphologies was studied. The SEM images of SGO-M6, SGO-M16 and SGO-M28, which were the samples obtained only by alkaline deposition are shown in Fig. 3 (a), (c) and (e) respectively. The flake size of the original GO was 32.9 □m at D90, 16.6 □m at D50 and 6.63 □m at D10 from the information provided by the manufacturer of the GO. Regarding th~~eis~~ information of GO, the flake size of about 20 □m which can be seen in the middle of the image of SGO-M6 in Fig.3 (a) was one GO flake. Sulfur covered the surface of the

GO flake judging from the EDX mapping for the magnified image of SGO-M6 (Fig. S4). SGO-M6 had about 40% sulfur content from the elemental analysis shown in Fig. 2 (a). Thus, the morphology of SGO-M6 kept the shape of the GO flakes as sulfur was covering the surface of GO. In this sample, the sulfur seemed not to be crystalized as independent particles. In Fig. 3 (c) for the image of SGO-M16 having about 55% sulfur content, the reduced GO flakes were more wrinkled. In the image, among the GO flakes, a morphology like that of a honey comb can be seen. These are the sulfur particles of which the surface was damaged by the electron beam of the SEM. The actual sulfur particles had a rough surface and immediately started to become like a honey comb after focusing the SEM. ~~Even though the parameters for the SEM measurement were adjusted, some damage could not be avoided to get clear images.~~ Considering this fact, sulfur crystalizing as bulk particles was observed in between the wrinkled reduced GO flakes in SGO-M16 in Fig. 3 (c). In Fig. 3 (e) of SGO-M28, the sulfur particles in between reduced GO flakes became much bigger and the reduced GO became less flaky. The images for SGO-M1 and SGO-M3 (see Fig. S5 (a) and (c)) showed similar morphology to that of SGO-M6 ~~in which reduced GO had some sulfur coverage on the surface maintaining the flakey shape of GO~~. The image of SGO-M52 (see Fig. S5 (e)) showed larger sulfur particles than SGO-M28 as expected. These observations indicate that the following process occurred during the alkaline deposition. At the beginning, sulfur started to deposit on the surface of GO. As the sulfur content increased, sulfur started to crystalize to create independent sulfur particles making the GO flakes wrinkle. Then the independent sulfur particles grew to be bigger chunks during the extended time.

SGO-Mx-Ay (x: alkaline deposition time, y: acidic deposition temperature) samples were prepared by acidic deposition following alkaline deposition for different times. The SEM images of SGO-M6-A15, SGO-M16-A15 and SGO-M28-A15 are shown in Fig. 3 (b), (d) and (f), which

correspond to SGO-M6 in Fig. 3 (a), SGO-M16 in Fig. 3 (c) and SGO-M28 in Fig. 3 (e) respectively. The image of SGO-M1-A15 and SGO-M3-A15 are also shown in Fig. S5. In the images of ~~SGO-M1-A15, SGO-M3-A15 and~~ SGO-M6-A15, very fine structures in the size range of 0.5 μm to 1.0 μm with wrinkled flaky shapes of GO and without independent agglomeration of sulfur were observed. These structures were confirmed to be composites of sulfur and GO judging from the EDX mapping results. It is surprising that these morphologies were significantly different from the morphology before acidification only with alkaline deposition such as SGO-M1, SGO-M3 and SGO-M6. Considering the fact that much of the polysulfide was still remaining in the mixture solution of polysulfide and GO before 6 hours mixing, those polysulfides deposited as sulfur to create the fine structure.

The reason for the structure difference between the samples resulting from alkaline deposition and from acidic deposition is presumed to be the reaction rate for sulfur deposition. The deposition rate in the alkaline deposition is much slower than that in the acidic deposition. If the reaction rate is slow, sulfur tends to deposit onto pre-existing crystals creating independent particles rather than distributed over the surface of the GO. Although sulfur deposited on the surface of GO at the beginning, once sulfur started to crystalize by itself, the sulfur crystals grew as more sulfur deposited. On the other hand, when the deposition rate is fast under the acidic condition, the collision frequency would be more dominant than stabilization. As a result, sulfur deposited on the surface of GO homogeneously rather than agglomerating. When the alkaline deposition time was longer, more polysulfide was already crystalized as sulfur particles of around 10 μm, and a smaller amount of polysulfide remained in the solution before acidification. Although similar fine structures like SGO-M6-A15 were observed in the morphology of SGO-M16-A15 in Fig. 3 (d), it seemed to have secondary particles of around 10 μm size.~~.~~ When the

alkaline deposition time was longer, more polysulfide was already crystalized as sulfur particles of around 10 μm, and a smaller amount of polysulfide remained in the solution before acidification. It can be supposed that the remaining polysulfide deposited as fine composites with GO in a fast reaction during the acidic deposition and surrounded the pre-existing bigger sulfur particles. From this mechanism, it is understandable that big sulfur particles in SGO-M28-A15 were not surrounded by fine structures of GO as shown in Fig. 3 (f) due to a smaller amount of remaining polysulfide. From these observations, it can be concluded that the remaining polysulfide after alkaline deposition created fine composites with GO flakes and surrounded the pre-existing sulfur particles during acidic deposition.

It was also found that acidic deposition conditions affected the morphologies of the samples. SEM images of SGO-M16-Ay (y: acidic deposition temperature) prepared by acidification at 5 °C, 15 °C and 25 °C are shown in Fig. 4 (a), (c) and (e) respectively. When the temperature during acidic deposition was 5 °C, the surfaces of the particles were covered by a very fine flaky structure as shown in Fig. 4 (a). On the other hand, as the temperature increased, the surface became more solid and insulating judging from the charging effects as shown in Fig. 4 (c). These indicate that GO was more on the surface of the composite for the low temperature acidic deposition, and sulfur was more on the surface of the composite when the temperature was high during the process. From the consideration about the influence of temperature on the acidic deposition time as seen in Fig. 2 (d), the deposition rate of sulfur was low as the acidic deposition temperature was low. From these results, it is assumed that the morphologies are affected by the reaction rate of sulfur deposition, which means that sulfur deposits more on the surface of the composite when the deposition rate is high at high temperature, and sulfur deposits inside the GO flaky structure when the deposition rate is low at low temperature. This

phenomenon is understandable from the fact that SGO-M16-Ay had bulk sulfur cores inside the flaky structures considering the morphology before the acidic deposition as seen in Fig. 3 (c). Then during the acidic deposition, polysulfide preferred to deposit as sulfur on the inner bulk sulfur surface rather than GO flakes at low temperature. ~~As a result, sulfur deposition occurred inside the flaky structure at low temperatures.~~ On the other hand, sulfur deposited on the surfaces which were easily reachable when the reaction rate was high at high temperature. From these discussions, the summary of the relationship between the conditions of the process and the resulting morphology are shown in Fig. 1 (b). As the alkaline deposition time becomes longer, more bulk sulfur particles are created by the slow sulfur deposition rate. When sulfur is deposited by acidic deposition, the sulfur deposits on GO to create a fine structure. But even in acidic deposition, if the temperature is low and some sulfur bulk particles pre-exist because of the alkaline deposition process, sulfur deposits on the pre-existing sulfur particles rather than the GO surface.

Heat treatment at 155 °C followed the acidic deposition process. The sulfur contents of all the samples after the heat treatment were the same as before the heat treatment, as checked by elemental analysis, and~~which~~ was 84%. SEM images of the samples after the heat treatment, SGO-M16-A5-H, SGO-M16-A15-H and SGO-M16-A25-H, are shown in Fig. 4 (b), (d) and (f) corresponding to the samples before the heat treatment shown in Fig. 4 (a), (c) and (e) respectively. It can be expected that sulfur melts during the heat treatment and redistributes itself in the composite. However, the main features of the morphologies of the samples were maintained even after the heat treatment at 155 °C for 18 hours. This means that the morphologies of the composites were largely determined by the alkaline deposition process and the acidic deposition process. Just what was noticed about the difference before and after the heat

treatment was that the sulfur parts were not fragile against the electron beam for SEM observation anymore. This is supposed from the analytical results in the previous study [7], which elucidated that a new layer was created on the composites after the heat treatment by the reactions of polysulfide and the cetyltrimethylammonium cation (CTA^+) produced from CTAB. This newly created layer was necessary to enhance the capacity maintenance of the cell using the sulfur/GO composite as the sulfur electrode active material [7].

The electrochemical performance of the samples prepared under different conditions was measured. The voltage profiles in the second cycle of SGO-M1-A15-H, SGO-M3-A15-H, SGO-M6-A15-H, SGO-M16-A15-H, SGO-M28-A15-H and SGO-M52-H, which were obtained using different alkaline deposition times, are shown in Fig. 5 (a). Only sample SGO-M52-H was prepared without acidic deposition because all the polysulfide was converted to sulfur during the long alkaline deposition. All the other samples were acidified, taking different times for all the polysulfide to be converted to sulfur after the different alkaline deposition times. All samples were heat-treated at 155 °C. SGO-M1-A15-H, SGO-M3-A15-H and SGO-M6-A15-H showed similar voltage profiles and capacities. This is reasonable judging from the similar morphologies in these materials as shown in Fig. 3 (b) and Fig. S6 (b) and (d). These were prepared by short alkaline deposition resulting in more than 60% of the sulfur deposited by acidic deposition. Meanwhile, SGO-M16-A15-H showed the highest capacity among the samples. In this material, 57% of the sulfur was deposited during the alkaline deposition and the rest of the sulfur deposited by the acidic deposition. SGO-M28-A15-H and SGO-M52-H showed lower capacities than SGO-M16-A15-H. About 70% of sulfur deposited by the alkaline deposition in the case of SGO-M28-A15-H, and 100% of the sulfur was accumulated by the alkaline deposition in the case of SGO-M52-H. ~~As shown in Fig. 3 (e) for SGO-M28 and Fig. S5 (e) for SGO-M52, these~~

~~materials had big agglomerations of sulfur because of the slow crystallization in the alkaline deposition.~~

From these results, it can be concluded that a specific combination of alkaline deposition and acidic deposition leads to high performance of the cathode active material. If too much sulfur deposits by acidic deposition like SGO-M1-A15-H, SGO-M3-A15-H and SGO-M6-A15-H, insulating sulfur covers the surface of GO as thick layers resulting in less conductivity of the materials. Less reduced GO also results in less conductivity. On the other hand, if too much sulfur is produced by alkaline deposition like SGO-M28-A15-H and SGO-M52-H, sulfur agglomerates in the slow process so that these big chunks of sulfur prevent the electron transfer to the inner sulfur in the particles.

Next, voltage profiles of SGO-M16-A5-H, SGO-M16-A10-H, SGO-M16-A15-H, SGO-M16-A20-H and SGO-M16-A25-H, which were prepared using different acidic deposition temperatures, are compared in Fig. 5 (b). SGO-M16-A5-H prepared at 5 °C acidic deposition showed a significantly higher capacity than the other samples. The capacity decreased in the order of increase in the acidic deposition temperature. It is surprising that the difference was critical. The voltage profiles for the first five cycles of SGO-M16-A5-H are shown in Fig. S7. The rate capabilities of samples with different preparation conditions were examined and showed in Fig. 6 (a). SGO-M16-A5-H showed the highest capacity at various C rates. The voltage profiles for each C rate of SGO-M16-A5-H are shown in Fig. 6 (b). The voltage profile after 100 cycles is shown in Fig. 6 (b) as well. The specific capacity remained at 800 mAh/g (sulfur) even after 150 cycles at 0.5 C discharge. Considering the morphologies in Fig. 4, better conductivity was provided for most sulfur by the surrounding flaky layer of reduced GO in SGO-M16-A5-H prepared at 5 °C acidic deposition temperature, whereas too much sulfur accumulation on the

surface of GO interfered with the conductivity among the particles for the composites prepared at higher acidic deposition temperatures. Thus, it can be concluded that a lower acidification temperature i.e. 5 °C was preferable for obtaining high capacity.

Considering these results together with the morphology of each sample, the relationships are illustrated in Fig. 1 (b). Too much sulfur agglomeration by too long alkaline deposition time caused loss of capacity due to isolation of inner sulfur deep inside the particles. On the other hand, if too much sulfur is deposited on the surface of GO only by acidic deposition without the alkaline deposition, or by high temperature acidic deposition even with the alkaline deposition, the conductivity on the surface of the composites was lost resulting in poor electronic conductivity among the particles. Thus, it was concluded that the specific combination of moderate alkaline deposition and acidic deposition at low temperatures led to the highest capacity of the cells using the composite as the sulfur electrode active material.

4. Conclusions:

The sulfur deposition process in the preparation of SGO nano-composite active material was carefully investigated. It was found that just mixing of a polysulfide solution and a GO suspension produced a composite of sulfur and reduced GO by alkaline deposition. Also, the acidification of the polysulfide solution by formic acid, i.e. acidic deposition was influenced significantly by temperature. The sulfur deposition rate under different conditions influenced the morphology of the materials and their resulting cell performance. By controlling the synthesis condition such as the combination of moderate alkaline deposition for 60% of the sulfur and the subsequent acidic deposition at a low temperature, specifically 5 °C, the preferred morphology of

the sulfur/GO composite with high capacity was successfully synthesized. This work should allow the controlled synthesis of SGO active material for high-performance Li/S cells.

ACKNOWLEDGMENT

We thank Tevye Kuykendall of the Molecular Foundry of LBNL for his generous support. Work at the Molecular Foundry was supported by the Office of Science, Office of Basic Energy Sciences, of the U.S. Department of Energy under Contract No. DE-AC02-05CH11231. We thank Elena Kreimer of the Microanalytical Facility in the College of Chemistry, Univerisity of California, Berkeley for her support.

FUNDING: This work was supported by ZAF Energy Systems

REFERENCES

[1] M.-K. Song, Y. Zhang, E. J. Cairns, A Long-Life, High-Rate Lithium/Sulfur Cell, A Multifaceted Approach to Enhancing Cell Performance, *Nano Lett.,* **13,** 5891-5899 (2013).

[2] L. Ji, M. Rao, H. Zheng, L. Zhang, Y. Li, W. Duan, J. Guo, E. J. Cairns, Y. Zhang, Graphene Oxide as a Sulfur Immobilizer in High Performance Lithium/Sulfur Cells, *J. Am. Chem. Soc.*, **133,** 18522-18525 (2011).

[3] L. Zhang, L. Ji, P.-A. Glans, Y. Zhang, J. Zhu, J. Guo, Electronic structure and chemical bonding of a graphene oxide–sulfur nanocomposite for use in superior performance lithium–sulfur cells, *Phys. Chem. Chem. Phys.*, **14**, 13670-13675 (2012).

[4] X. Feng, M.-K. Song, W. C. Stolte, D. Gardenghi, D. Zhang, X. Sun, J. Zhu, E. J. Cairns, J. Guo, Understanding the degradation mechanism of rechargeable lithium/sulfur cells: a comprehensive study of the sulfur–graphene oxide cathode after discharge–charge cycling, *Phys.*

Chem. Chem. Phys., **16**, 16931-16940 (2014).

[5] Y. Ye, A. Kawase, M. Song, B. Feng, Y. Liu, M. A. Marcus, J. Feng, E. J. Cairns, J. Guo, J. Zhu, X-ray Absorption Spectroscopy Characterization of a Li/S Cell, *Nanomaterials*, **6**, doi:10.3390/nano6010014 (2016).

[6] Y. Ye, A. Kawase, M. Song, B. Feng, Y. Liu, M. A. Marcus, J. Feng, H. Fang, E. J. Cairns, J. Guo, J. Zhu, X-ray Absorption Spectroscopic Characterization of the Synthesis Process: Revealing the Interactions in Cetyltrimethylammonium Bromide-Modified Sulfur−Graphene Oxide Nanocomposites, *J. Phys. Chem. C*, **120**, 10111-10117 (2016).

[7] A. Kawase, E. J. Cairns. Understanding the function of cetyltrimethyl ammonium bromide in Lithium/Sulfur Cells, *J. Mater. Chem. A*, DOI: 10.1039/C7TA07522G (2017).

[8] Z. Wang, Y. Dong, H. Li, Z. Zhao, H. B. Wu, C. Hao, S. Liu, J. Qiu, X. W. (D.) Lou, Enhancing lithium–sulphur battery performance by strongly binding the discharge products on amino-functionalized reduced graphene oxide, *Nat. Commun*., doi: 10.1038/ncomms6002 (2014).

[9] C. Zu, A. Manthiram, Hydroxylated Graphene–Sulfur Nanocomposites for High-Rate Lithium–Sulfur Batteries, *Adv. Energy Mater*., **3**, 1008–1012 (2013).

[10] L. Q. Lu, L. J. Lu, Y. Wang, Sulfur film-coated reduced graphene oxide composite for lithium–sulfur batteries, *J. Mater. Chem. A*, **1**, 9173-9181 (2013).

[11] F. Zhang, X. Zhang, Y. Dong, L. Wang, Facile and effective synthesis of reduced graphene oxide encapsulated sulfur via oil/water system for high performance lithium sulfur cells. *J. Mater. Chem.*, **22**, 11452-11454 (2012).

[12] H. Sun, G. Xu, Y. Xu, S. Sun, X. Zhang, Y. Qiu, S. Yang, A Composite Material of Uniformly Dispersed Sulfur on Reduced Graphene Oxide: Aqueous One-Pot Synthesis,

Characterization. *Nano Res*., **5**, 726–738 (2012).

[13] J. Rong, M. Ge, X. Fang, C. Zhou, Solution Ionic Strength Engineering As a Generic Strategy to Coat Graphene Oxide (GO) on Various Functional Particles and Its Application in High-Performance Lithium−Sulfur (Li−S) Batteries. *Nano Lett*., **14**, 473−479 (2014).

[14] H. Wang, Y. Yang, Y. Liang, J. T. Robinson, Y. Li, A. Jackson, Y. Cui, H. Dai, Graphene-Wrapped Sulfur Particles as a Rechargeable Lithium Sulfur Battery Cathode Material with High Capacity and Cycling Stability. *Nano Lett*., **11**, (7), 2644–2647 (2011).

[15] A. Teder, The equilibrium between elemental sulfur and aqueous polysulfide solutions. *Acta Chem. Scand.*, **25**, 1722-1728 (1971).

[16] F. Barroso-Bujans, A. Alegrı´a, J. Colmenero, Kinetic Study of the Graphite Oxide Reduction: Combined Structural and Gravimetric Experiments under Isothermal and Nonisothermal Conditions. *J. Phys. Chem. C*, **114**, 21645–21651 (2010).

[17] A. M. Dimiev, L. B. Alemany, J. M. Tour, Graphene Oxide. Origin of Acidity, Its Instability in Water, and a New Dynamic Structural Model. *ACS Nano*, **7**, 576-588 (2013).

[18] R. Steudel, Mechanism for the Formation of Elemental Sulfur from Aqueous Sulfide in Chemical and Microbiological Desulfurization Processes. *Ind. Eng. Chem. Res.*, **35**, 1417-1423 (1996).

[19] T. Warnheim, A. Jonsson, Phase Diagrams of Alkyltrimethylammonium Surfactants in Some Polar Solvents, *J. Colloid Interface Sci*., **125**, 627-633 (1988).

Table 1. List of samples prepared in different synthesis condition.

Sample	Alkaline deposition time	Acidic deposition temperature	Heat treatment
SGO-M1	1 hour	None	None

SGO-M3	3 hours	None	None
SGO-M6	6 hours	None	None
SGO-M16	16 hours	None	None
SGO-M28	28 hours	None	None
SGO-M52	52 hours	None	None
SGO-M1-A15	1 hour	15 °C	None
SGO-M3-A15	3 hours	15 °C	None
SGO-M6-A15	6 hours	15 °C	None
SGO-M16-A5	16 hours	5 °C	None
SGO-M16-A15	16 hours	15 °C	None
SGO-M16-A20	16 hours	20 °C	None
SGO-M16-A25	16 hours	25 °C	None
SGO-M28-A15	28 hours	15 °C	None
SGO-M1-A15-H	1 hour	15 °C	155 °C 18 hours
SGO-M3-A15-H	3 hours	15 °C	155 °C 18 hours
SGO-M6-A15-H	6 hours	15 °C	155 °C 18 hours
SGO-M16-A5-H	16 hours	5 °C	155 °C 18 hours
SGO-M16-A15-H	16 hours	15 °C	155 °C 18 hours
SGO-M16-A20-H	16 hours	20 °C	155 °C 18 hours
SGO-M16-A25-H	16 hours	25 °C	155 °C 18 hours
SGO-M28-A15-H	28 hours	15 °C	155 °C 18 hours
SGO-M52-H	52 hours	None	155 °C 18 hours

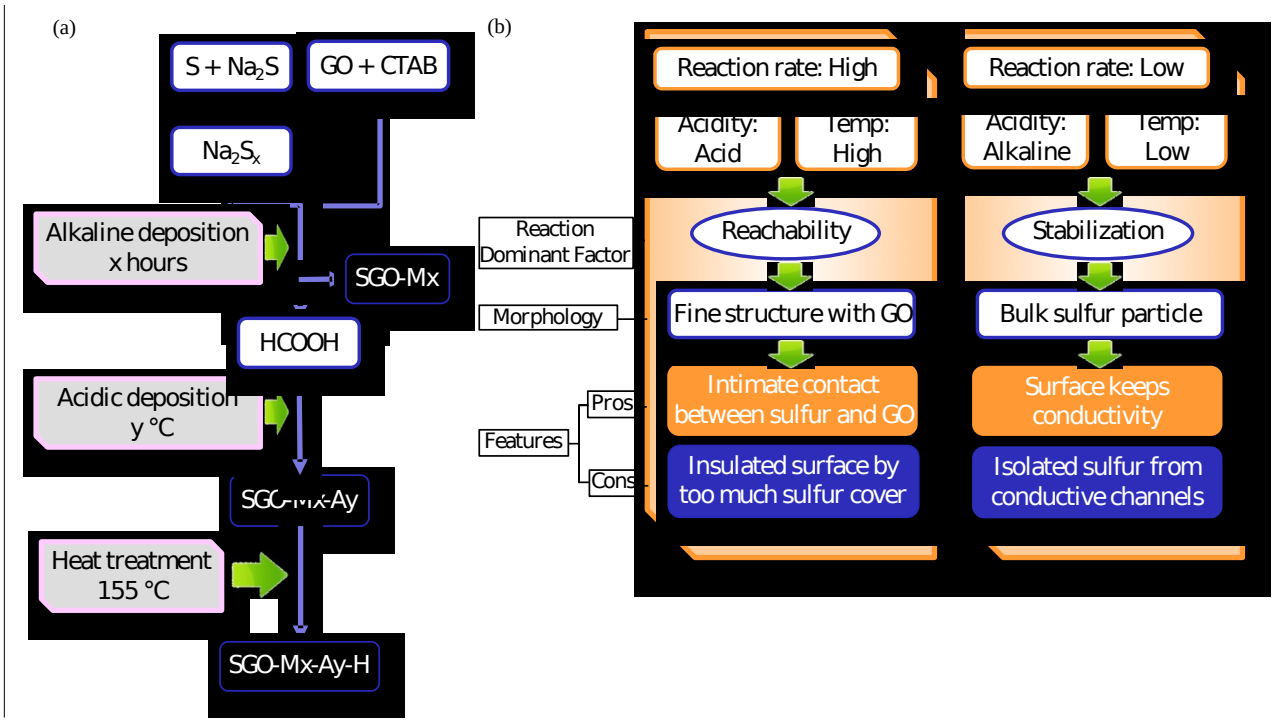
(a)
S + Na2S
GO + CTAB
Na2Sx
Alkaline deposition
x hours
SGO-Mx
HCOOH
Acidic deposition
y °C
SGO-Mx-Ay
Heat treatment
155 °C
SGO-Mx-Ay-H
(b)
Reaction Dominant Factor
Morphology
Features
Pros
Cons
Reaction rate: High
Acidity: Acid
Temp: High
Reachability
Fine structure with GO
Intimate contact between sulfur and GO
Insulated surface by too much sulfur cover
Reaction rate: Low
Acidity: Alkaline
Temp: Low
Stabilization
Bulk sulfur particle
Surface keeps conductivity
Isolated sulfur from conductive channels

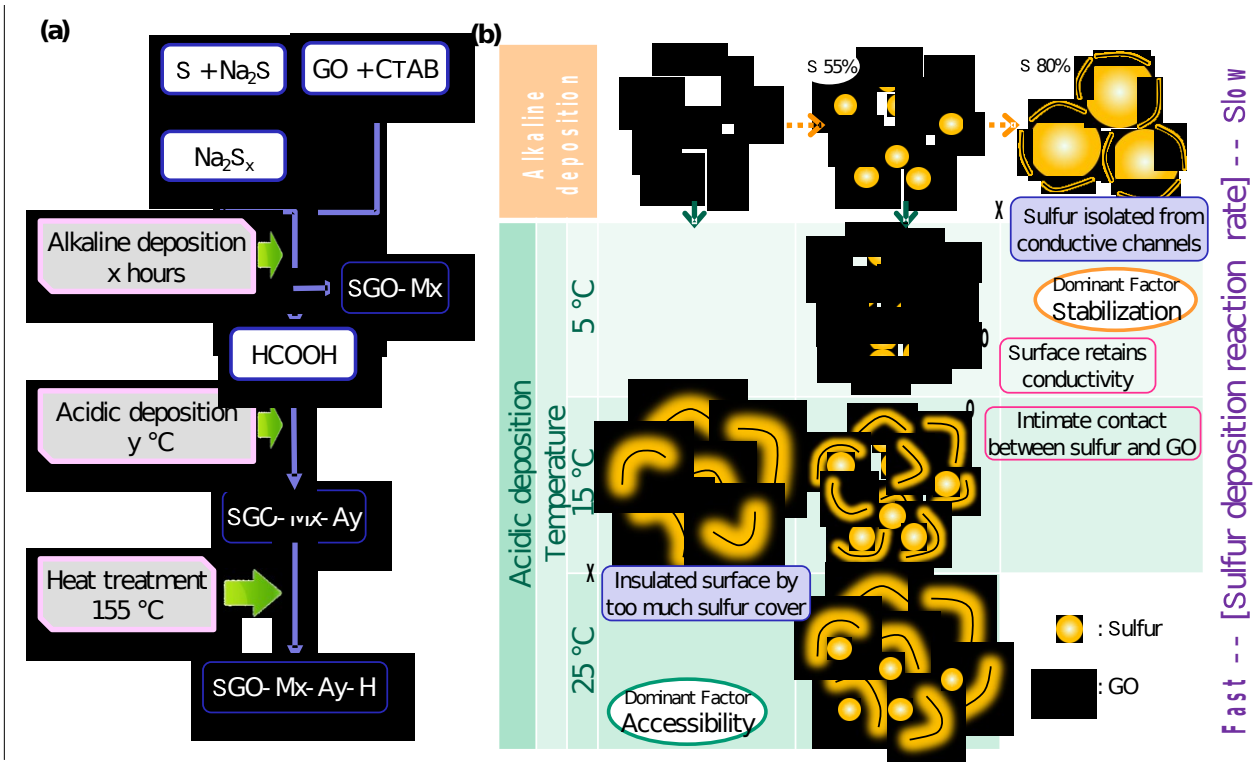

Fig. 1 Graphical explanation of the preparation and summary

(a) Diagram of the preparation of the sulfur/GO composite. (b) Summary of the relationship between the processing conditions and the resulting morphology.

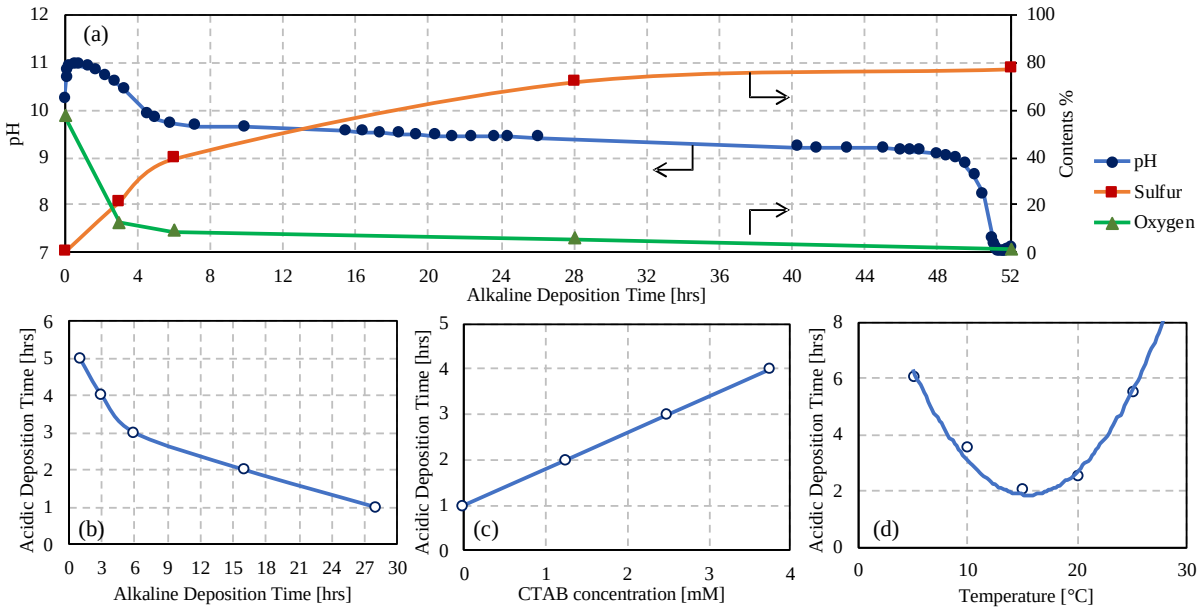

Fig. 2. Various parameter changes during the synthesis

(a) The contents of sulfur and oxygen in SGO-Mx (x is variable for the alkaline deposition time) samples and the pH change of the Na_2S_x-GO-CTAB mixture solution. (b) Acidic deposition times for different alkaline deposition times. (c) Acidic deposition times for different CTAB concentrations in the mixture solutions. (d) Temperature dependency of the acidic deposition time.

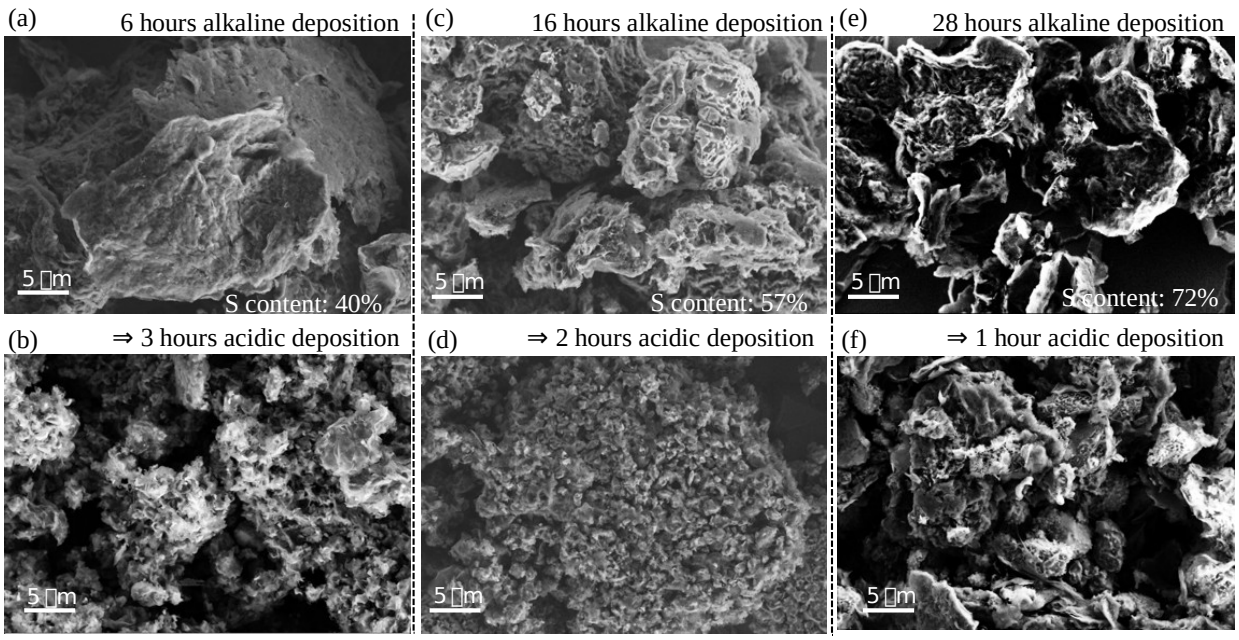
(a)
6 hours alkaline deposition
5 μm
S content: 40%
(c)
16 hours alkaline deposition
5 μm
S content: 57%
(e)
28 hours alkaline deposition
5 μm
S content: 72%
(b)
⇒ 3 hours acidic deposition
5 μm
(d)
⇒ 2 hours acidic deposition
5 μm
(f)
⇒ 1 hour acidic deposition
5 μm

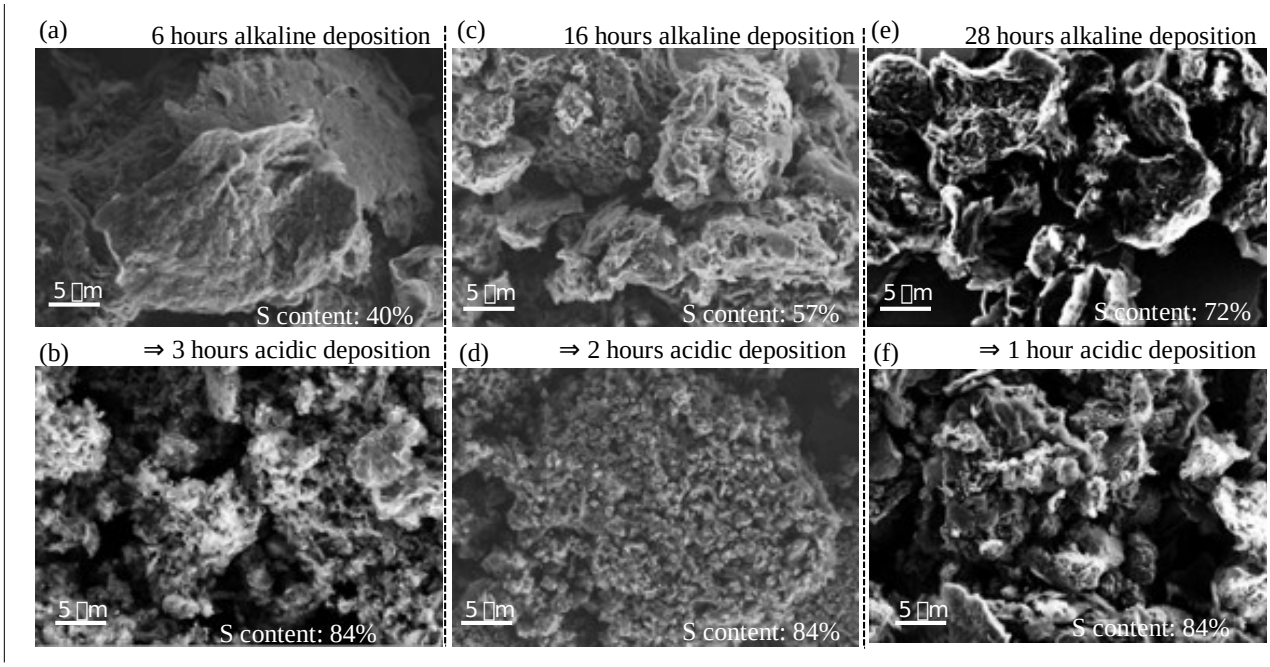

Fig. 3. SEM images for samples prepared in different processing times

SEM images of SGO-M6 (a), SGO-M16 (c) and SGO-M28 (e), which were the samples obtained only by alkaline deposition, and SGO-M6-A15 (b), SGO-M16-A15 (d) and SGO-M28-A15 (f), which were obtained after subsequent acidic deposition for SGO-M6, SGO-M16 and SGO-M28 respectively.

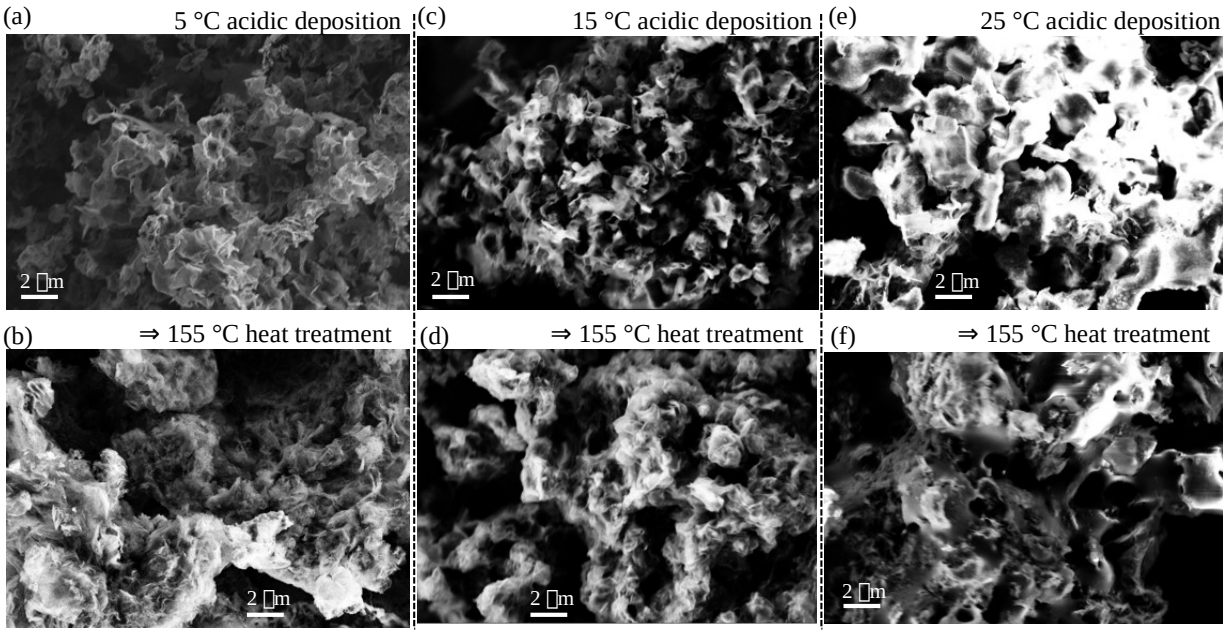

Fig. 4. SEM images for samples prepared in different acidification temperatures

SEM images of SGO-M16-A5 (a), SGO-M16-A15 (c) and SGO-M16-A25 (e), which were the samples before the heat treatment, and SGO-M16-A5-H (b), SGO-M16-A15-H (d) and SGO-M16-A25-H (f), which were obtained after subsequent heat treatment of SGO-M16-A5, SGO-M16-A15 and SGO-M16-A25 respectively.

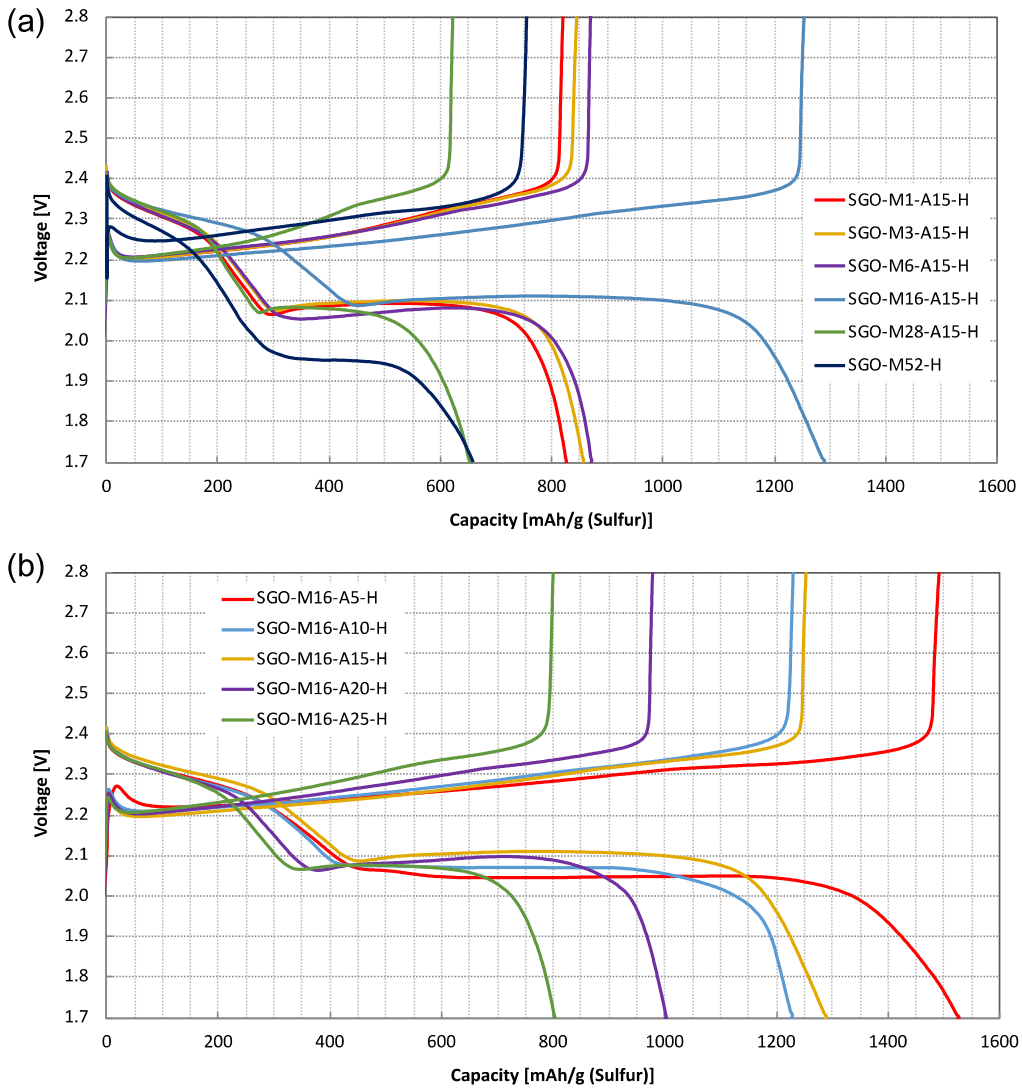

Fig. 5. Cell performance

(a) The voltage profiles in the second cycle of SGO-M1-A15-H, SGO-M3-A15-H, SGO-M6-A15-H, SGO-M16-A15-H, SGO-M28-A15-H and SGO-M52-H, which were obtained using different alkaline deposition times. (b) The voltage profiles of SGO-M16-A5-H, SGO-M16-A10-H, SGO-M16-A15-H, SGO-M16-A20-H and SGO-M16-A25-H, which were prepared using different acidic deposition temperatures.

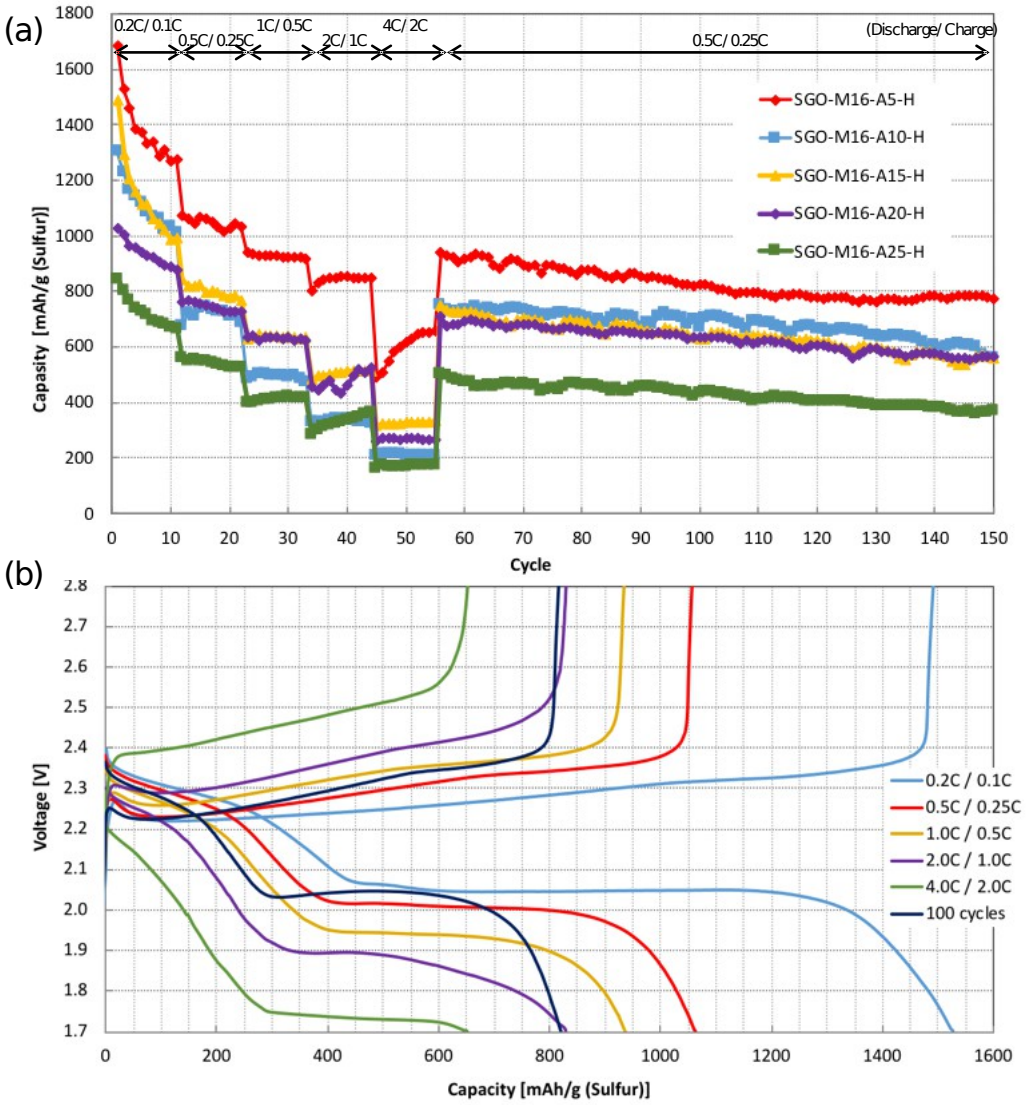

Fig. 6. Rate capability and cycle

(a) The rate capabilities and the cycle performance of SGO-M16-A5-H, SGO-M16-A10-H, SGO-M16-A15-H, SGO-M16-A20-H and SGO-M16-A25-H, which were prepared using different acidic deposition temperatures. (b) The voltage profile of SGO-M16-A5-H for different C rates and after 100 cycles.